

Learning Fine-Grained Geometry for Sparse-View Splatting via Cascade Depth Loss

Wenjun Lu
The University of Sydney
Sydney, NSW, Australia
wenjun.lu@sydney.edu.au

Haodong Chen
The University of Sydney
Sydney, NSW, Australia
haodong.chen@sydney.edu.au

Anqi Yi
The University of Sydney
Sydney, NSW, Australia
anqi.yi@sydney.edu.au

Yuk Ying Chung
The University of Sydney
Sydney, NSW, Australia
vera.chung@sydney.edu.au

Zhiyong Wang
The University of Sydney
Sydney, NSW, Australia
zhiyong.wang@sydney.edu.au

Kun Hu
Edith Cowan University
Perth, Western Australia, Australia
k.hu@ecu.edu.au

Abstract

Novel view synthesis is a fundamental task in 3D computer vision that aims to reconstruct realistic images from a set of posed input views. However, reconstruction quality degrades significantly under sparse-view conditions due to limited geometric cues. Existing methods, such as Neural Radiance Fields (NeRF) and the more recent 3D Gaussian Splatting (3DGS), often suffer from blurred details and structural artifacts when trained with insufficient views. Recent works have identified the quality of rendered depth as a key factor in mitigating these artifacts, as it directly affects geometric accuracy and view consistency. In this paper, we address these challenges by introducing Hierarchical Depth-Guided Splatting (HDGS), a depth supervision framework that progressively refines geometry from coarse to fine levels. Central to HDGS is a novel Cascade Pearson Correlation Loss (CPCL), which aligns rendered and estimated monocular depths across multiple spatial scales. By enforcing multi-scale depth consistency, our method substantially improves structural fidelity in sparse-view scenarios. Extensive experiments on the LLFF and DTU benchmarks demonstrate that HDGS achieves state-of-the-art performance under sparse-view settings while maintaining efficient and high-quality rendering.

CCS Concepts

• Computing methodologies → Rendering.

Keywords

Novel View Synthesis, Real-time Rendering, 3D Gaussian Splatting

ACM Reference Format:

Wenjun Lu, Haodong Chen, Anqi Yi, Yuk Ying Chung, Zhiyong Wang, and Kun Hu. 2025. Learning Fine-Grained Geometry for Sparse-View Splatting via Cascade Depth Loss. In *Proceedings of Make sure to enter the correct conference title from your rights confirmation email (Conference acronym 'XX)*. ACM, New York, NY, USA, 10 pages. <https://doi.org/XXXXXXX.XXXXXXX>

Permission to make digital or hard copies of all or part of this work for personal or classroom use is granted without fee provided that copies are not made or distributed for profit or commercial advantage and that copies bear this notice and the full citation on the first page. Copyrights for components of this work owned by others than the author(s) must be honored. Abstracting with credit is permitted. To copy otherwise, or republish, to post on servers or to redistribute to lists, requires prior specific permission and/or a fee. Request permissions from permissions@acm.org.
Conference acronym 'XX, Woodstock, NY

© 2025 Copyright held by the owner/author(s). Publication rights licensed to ACM.
ACM ISBN 978-x-xxxx-xxxx-x/YYYY/MM
<https://doi.org/XXXXXXX.XXXXXXX>

1 Introduction

Reconstructing photorealistic images of a scene from novel view-points, commonly referred to as novel view synthesis (NVS), is a fundamental problem in 3D computer vision. It supports a wide range of applications including virtual and augmented reality, autonomous navigation, and robotic perception. These use cases often require high-quality renderings from previously unseen perspectives, making the ability to synthesize novel views both technically critical and practically valuable.

State-of-the-art NVS methods such as Neural Radiance Fields (NeRF) [21] and the more recent 3D Gaussian Splatting (3DGS) [14] have shown impressive results under dense view supervision. NeRF represents the scene implicitly using multilayer perceptrons (MLPs), producing high-fidelity images but suffering from long training and inference times. In contrast, 3DGS models the scene explicitly as a set of anisotropic 3D Gaussians, allowing real-time rendering while maintaining visual quality in dense view settings.

However, both Neural Radiance Fields (NeRF) and 3D Gaussian Splatting (3DGS) experience significant performance degradation when trained with limited input views. In real-world scenarios such as large-scale outdoor environments, complex indoor scenes with frequent occlusions, or mobile capture setups constrained by time, hardware, or cost, collecting dense multi-view image data is often impractical. As a result, models receive insufficient geometric cues, which severely hampers their ability to accurately reconstruct scene structure and appearance.

In these sparse-view conditions, NeRF's reliance on dense photometric supervision becomes a major limitation. The model struggles to resolve spatial ambiguity, often producing artifacts and inconsistent geometry due to its inability to infer complete 3D information from limited observations. Similarly, 3DGS, which explicitly represents scenes using a set of 3D Gaussian primitives, depends on reliable initialization and comprehensive coverage to correctly optimize the position and scale of each primitive.

The problem is further intensified in 3DGS by the inherent smoothing behavior of Gaussian kernels. When geometric constraints are weak, the spatially continuous nature of Gaussians leads to excessive blending between primitives. This effect can blur object boundaries, suppress high-frequency details, and reduce the overall sharpness of the rendered output. Moreover, without sufficient views, the model is prone to overfitting to the training

images, which significantly diminishes its ability to generalize to novel viewpoints.

Recent approaches [8, 24, 37, 45] have attempted to address this problem by incorporating monocular depth priors to provide additional geometric supervision. These priors offer useful constraints without requiring extra input views. However, most existing methods apply depth alignment at a fixed global scale. This often leads to inaccurate scene representation as the model fails to capture important local structural variations. Although methods such as DNGaussian have investigated patch-level depth alignment, they do not employ correlation-based supervision between rendered and predicted depth distributions which restricts their capacity to capture structural consistency.

To address these limitations, we propose a method called **Hierarchical Depth-Guided Splatting (HDGS)**, which enhances 3DGS in sparse-view settings through multi-scale depth supervision. Our key idea is to refine scene geometry progressively from coarse to fine levels by aligning rendered and predicted monocular depth maps at multiple spatial resolutions. This hierarchical structure allows the model to learn both the global scene layout and detailed local geometry, improving the placement and scaling of 3D Gaussians when input views are limited.

At the core of HDGS is a new loss function called **Cascade Pearson Correlation Loss (CPCL)**. This loss compares depth patches at various scales using Pearson correlation, a scale-invariant measure of structural similarity. The loss is applied in a cascade, where depth alignment begins at coarse resolution and progressively moves to finer levels. This structure-aware regularization enables more robust geometric learning, especially in the presence of depth noise, scene ambiguity, or missing regions in monocular predictions.

In addition to our depth supervision framework, we introduce two practical enhancements that further improve reconstruction quality. First, following insights from recent work [5], we replace the traditional Gaussian kernel used in 3DGS with a linear kernel. The linear kernel introduces sharper spatial boundaries and reduces excessive blending between neighboring Gaussians, which helps preserve high-frequency details. Second, we initialize the 3D point cloud using VGGSfM [33], which produces significantly denser and more reliable point clouds than the original sparse and noisy initialization used in 3DGS under limited views.

We evaluate our method on the LLFF and DTU benchmarks and show that HDGS achieves state-of-the-art performance in sparse-view novel view synthesis. Our approach improves both structural fidelity and visual quality while maintaining efficient and real-time rendering performance.

Our main contributions are as follows:

- **Hierarchical Depth Guided Splatting (HDGS):** We propose a multi-scale depth alignment framework that captures geometric consistency from the global scene to fine local details. This improves Gaussian placement under sparse-view conditions.
- **Cascade Pearson Correlation Loss (CPCL):** We introduce a correlation-based loss that progressively aligns rendered and predicted depths at multiple spatial resolutions. This cascading structure provides strong and stable supervision despite depth ambiguity or noise.

- **State-of-the-art Performance:** Our method achieves state-of-the-art results on standard sparse-view benchmarks including LLFF and DTU. It outperforms existing NeRF- and 3DGS-based methods in both reconstruction accuracy and visual quality.

2 Related Work

2.1 Radiance Fields for Novel View Synthesis

NeRF has significantly advanced the field of novel view synthesis, providing compact, implicit scene representations via Multi-layer Perceptrons. Unlike traditional explicit methods, such as point clouds, meshes, or voxel grids, NeRF models scenes implicitly by mapping spatial coordinates and view directions to color and density values. Following its success, numerous subsequent works expanded the NeRF framework to address limitations, including rendering quality[1, 2], robustness to pose estimation errors[15, 19, 31], handling dynamic or unbounded scenes[9, 26], and significantly accelerating both training and rendering times. For instance, InstantNGP[22] leverages multi-resolution hash encoding to shorten training periods from days to mere seconds drastically. However, despite these improvements, NeRF methods remain computationally intensive due to their requirement for dense volumetric sampling and expensive per-ray evaluations through multilayer perceptrons, limiting their practicality in real-time applications.

Following the development of implicit neural representations like NeRF, explicit scene representations have emerged. One of the most notable developments in this space is 3D Gaussian Splatting (3DGS), which models scenes using anisotropic 3D Gaussians rendered through differentiable splatting techniques. This approach contrasts with volumetric radiance fields that necessitate dense sampling and extensive MLP computations; instead, 3DGS facilitates direct and efficient rasterization, making it well-suited for real-time applications. The seminal work by Kerbl et al. [14] demonstrated that high-fidelity view synthesis could be achieved with significantly reduced training and inference times, inspiring subsequent research to enhance fidelity, robustness, and generalization. Comprehensive surveys[4, 34] have corroborated the efficacy of 3DGS in dense-view scenarios and underscored its adaptability to mobile and interactive applications. Compared to traditional mesh- or voxel-based explicit methods, 3DGS offers a more compact and smooth representation that inherently captures appearance and geometry without necessitating mesh connectivity or voxel discretization. Further advancements have focused on improving splatting-based differentiability, anisotropy modeling, and integration with neural priors[6, 18]. Efforts are also underway to extend 3DGS to broader scenarios, including dynamic scenes[13, 17], uncalibrated views[28, 36], and mixed-modality input[29, 30]. Additionally, recent work explores integrating signed distance functions into 3DGS to better enforce geometric fidelity at object boundaries [43]. However, despite its advanced reconstruction quality and rendering efficiency, 3DGS still faces significant challenges when applied to sparse-view image scenarios.

2.2 Sparse View Novel View Synthesis

Generating novel views from limited input images is inherently challenging due to the scarcity of geometric and appearance cues,

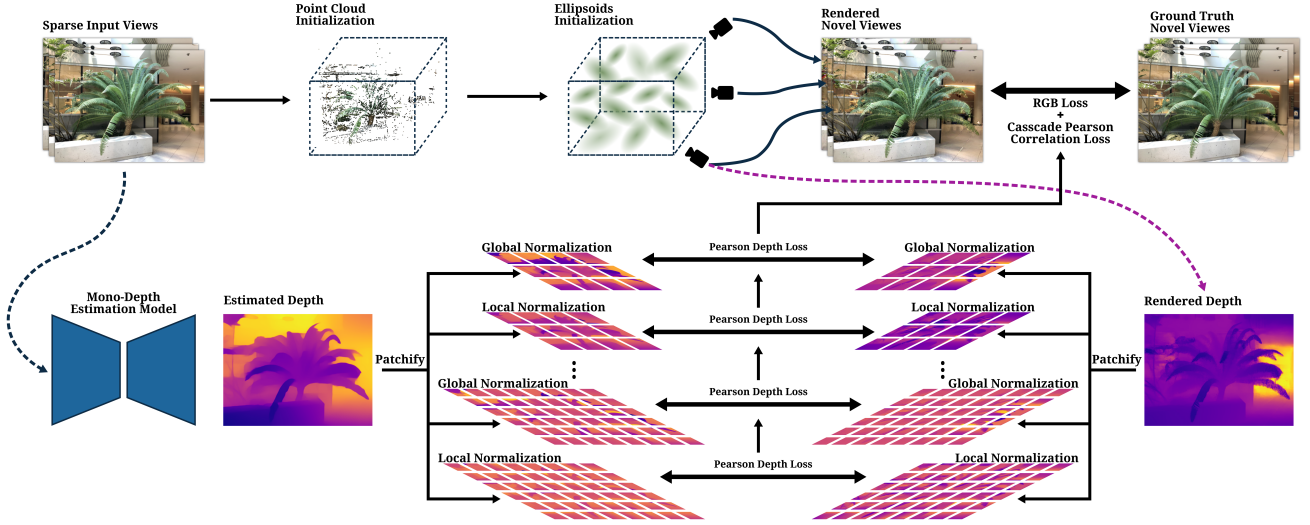


Figure 1: Overview of our framework: Given sparse input views, we initialize 3D Gaussians using a dense point cloud and supervise geometry via hierarchical alignment between rendered and monocular depth maps. A cascade Pearson correlation loss is applied across multi-scale patches and normalization modes, enabling accurate reconstruction under sparse-view conditions.

resulting in severe degradation and overfitting. To address this, several NeRF-based approaches introduce various regularization methods. RegNeRF[23] uses appearance regularization derived from normalizing flow models alongside depth smoothing to improve generalization. FreeNeRF[38] applies frequency constraints, mitigating high-frequency artifacts that typically result from overfitting. Furthermore, methods like Diet-NeRF[11] incorporate semantic consistency constraints using CLIP embeddings to enhance semantic coherence across views. SparseNeRF[32] improves geometric stability by introducing visibility-aware regularization that penalizes view-inconsistent structures. Nevertheless, these implicit volumetric methods still struggle with efficiency, limiting practical deployment in real-time settings.

CoR-GS[42] and Self-Ensembling gaussian splatting[44] methods train multiple Gaussian models with co-regularization strategies to mitigate overfitting and reduce rendering inconsistencies. While effective, these approaches introduce additional training overhead compared to simpler initialization or regularization-based methods. Techniques like Binocular gaussian splatting[10] and MVPGS[37] leverage multi-view priors to synthesize pseudo-ground truth for novel views, but these priors are often error-prone due to matching noise and geometric inaccuracies. Pretty much most of the existing methods include monocular depth to supervise model training—such as FSGS[45], CoherentGS[24], and DRGS[8]—but they typically rely on global-scale predictions that can suffer from scale inconsistencies and often neglect fine-grained local details. Although DNGaussian[16] have begun to incorporate local depth to better capture spatial detail, they still lack a structured mechanism to integrate depth information consistently across different scales. In contrast, our method introduces hierarchical depth supervision by integrating monocular depth cues at multiple granularities

enabling robust depth alignment that effectively addresses the limitations of prior monocular depth-based constraints.

3 Methods

Our proposed method as shown in Figure 1, Hierarchical Depth Guided Sparse-View 3D Gaussian Splatting, addresses the critical limitations observed in previous sparse-view reconstruction approaches. We utilize Linear kernel-based splatting to mitigate unwanted smoothing effects and preserve local geometric details effectively. Hierarchical depth supervision is employed to ensure accurate Gaussian placement by leveraging monocular depth information at multiple spatial scales—global, regional, and local. The Cascade Pearson Correlation loss robustly aligns rendered and monocular depth estimates across hierarchical scales. Furthermore, dense initialization via the VGGSfM model enhances the initial point cloud, leading to improved convergence and reconstruction quality. In this section, we detail each component comprehensively

3.1 Preliminary of 3D Gaussian Splatting

3D Gaussian Splatting (3DGS) explicitly represents a scene as a set of anisotropic Gaussian primitives. Each Gaussian is parameterized by a mean (center) position $\mu \in \mathbb{R}^3$, a covariance matrix $\Sigma \in \mathbb{R}^{3 \times 3}$, an opacity $\alpha \in \mathbb{R}$, and a color feature represented by spherical harmonics coefficients $\mathbf{c} \in \mathbb{R}^{3(l+1)^2}$, where l is the degree of spherical harmonics.

The influence of each Gaussian at a position $\mathbf{x} \in \mathbb{R}^3$ in 3D space is modeled as:

$$G(\mathbf{x}) = \exp\left(-\frac{1}{2}(\mathbf{x} - \mu)^T \Sigma^{-1}(\mathbf{x} - \mu)\right). \quad (1)$$

To ensure that Σ remains positive semi-definite and practically optimizable, it is decomposed into a rotation matrix $\mathbf{R} \in \mathbb{R}^{3 \times 3}$ and a diagonal scaling matrix $\mathbf{S} = \text{diag}(s_1, s_2, s_3) \in \mathbb{R}^{3 \times 3}$ as:

$$\Sigma = \mathbf{R}\mathbf{S}^2\mathbf{R}^\top. \quad (2)$$

During rendering, each Gaussian is projected from 3D world coordinates to 2D image coordinates using the camera's extrinsic matrix $\mathbf{T}_{wc} = [\mathbf{R}_{wc} | \mathbf{t}_{wc}] \in \text{SE}(3)$ and intrinsic matrix $\mathbf{K} \in \mathbb{R}^{3 \times 3}$. The mean and covariance in image space are computed as:

$$\boldsymbol{\mu}' = \pi(\mathbf{K}(\mathbf{R}_{wc}\boldsymbol{\mu} + \mathbf{t}_{wc})), \quad \Sigma' = \mathbf{J}\mathbf{R}_{wc}\Sigma\mathbf{R}_{wc}^\top\mathbf{J}^\top, \quad (3)$$

where $\pi(\cdot)$ denotes the perspective projection function, and $\mathbf{J} \in \mathbb{R}^{2 \times 3}$ is the Jacobian matrix of the affine approximation of the projection.

The final color $\mathbf{C}(\mathbf{p})$ at pixel $\mathbf{p} \in \mathbb{R}^2$ is computed by alpha blending all Gaussians that contribute to that pixel, sorted by their depth:

$$\mathbf{C}(\mathbf{p}) = \sum_i \alpha_i \mathbf{c}_i \prod_{j < i} (1 - \alpha_j), \quad (4)$$

where α_i is the visibility weight of the i -th Gaussian and \mathbf{c}_i is the view-dependent color

3.2 Linear Kernel-based 3D Splatting

In the standard 3D Gaussian Splatting (3DGS) framework, the influence of each point is modeled using a Gaussian kernel, which applies an exponential decay based on the Mahalanobis distance. This smooth falloff facilitates continuous surface blending but inherently suppresses fine geometric details—particularly problematic in sparse-view scenarios where high-frequency information is already limited.

To alleviate this, we replace the Gaussian kernel with a linear kernel that preserves the core structure of the 3DGS framework while modifying its attenuation behavior. Specifically, the Gaussian attenuation function:

$$G(\mathbf{x}) = \exp\left(-\frac{1}{2}D_M^2\right), \quad D_M = \sqrt{(\mathbf{x} - \boldsymbol{\mu})^\top \Sigma^{-1}(\mathbf{x} - \boldsymbol{\mu})}$$

is substituted with a linear attenuation function:

$$L(\mathbf{x}) = \max(0, 1 - D_M).$$

This modification retains the Gaussian center $\boldsymbol{\mu}$ and covariance matrix Σ , ensuring compatibility with existing accumulation and blending operations. However, the linear kernel sharply limits the spatial extent of each splat's influence, concentrating it within a finite radius defined by the Mahalanobis distance. As a result, the linear kernel produces crisper boundaries, reduces oversmoothing, and better preserves high-frequency content.

During rendering, each 3D Gaussian is projected into the 2D image space. The 2D version of the Mahalanobis distance is defined as:

$$D'_M = \sqrt{(\mathbf{x}' - \boldsymbol{\mu}')^\top \Sigma_{2D}^{-1}(\mathbf{x}' - \boldsymbol{\mu}')},$$

and the corresponding 2D linear kernel becomes:

$$L'(\mathbf{x}') = \max(0, 1 - D'_M).$$

By replacing the kernel function without altering the mathematical structure of splatting and blending, our method achieves sharper

reconstructions and enhanced detail preservation, especially in regions with intricate geometry or sparse viewpoint coverage.

$$K_{linear}(\mathbf{x}, \mathbf{x}_i) = \max\left(0, 1 - \frac{|\mathbf{x} - \mathbf{x}_i|}{r}\right) \quad (5)$$

where \mathbf{x} is the spatial coordinate being evaluated, \mathbf{x}_i is the kernel center, and r is the kernel radius.

3.3 Hierarchical Depth Supervision

To improve geometric reconstruction under sparse-view constraints, we propose a **Hierarchical Depth-Guided** mechanism that enforces consistency between the rendered depth $D_{rendered} \in \mathbb{R}^{1 \times H \times W}$ and the predicted monocular depth $D_{mono} \in \mathbb{R}^{1 \times H \times W}$ across multiple spatial resolutions. This multi-scale supervision scheme progressively aligns coarse scene geometry and fine-grained local structures, making it more robust to view sparsity and scale ambiguity.

We define a set of patch sizes $\mathcal{S} = \{s_1, s_2, \dots, s_N\}$ that represent varying levels of spatial granularity. For each scale $s \in \mathcal{S}$, we divide both depth maps into non-overlapping patches of size $s \times s$ via an unfolding operation. This process flattens each depth map $D \in \mathbb{R}^{1 \times H \times W}$ into patch sets:

$$\mathcal{P}_{rendered}^s = \text{Unfold}(D_{rendered}, s), \quad \mathcal{P}_{mono}^s = \text{Unfold}(D_{mono}, s),$$

$$\mathcal{P}_{rendered}^s = \{\mathbf{x}_1^r, \dots, \mathbf{x}_K^r\}, \quad \mathcal{P}_{mono}^s = \{\mathbf{x}_1^m, \dots, \mathbf{x}_K^m\},$$

where each $\mathbf{x}_k^r, \mathbf{x}_k^m \in \mathbb{R}^{s^2}$ represents the vectorized pixel values of the k -th patch and $K = \frac{H \cdot W}{s^2}$ is the number of patches per image at that scale.

3.3.1 Local Normalization. Local normalization focuses on internal patch structure while ignoring absolute depth scale. Each patch is normalized independently by subtracting its mean and dividing by its standard deviation:

$$\hat{\mathbf{x}}_k^r = \frac{\mathbf{x}_k^r - \mu(\mathbf{x}_k^r)}{\sigma(\mathbf{x}_k^r) + \epsilon}, \quad \hat{\mathbf{x}}_k^m = \frac{\mathbf{x}_k^m - \mu(\mathbf{x}_k^m)}{\sigma(\mathbf{x}_k^m) + \epsilon}.$$

This normalization removes local scale and bias effects, allowing the loss to focus purely on patch-wise structural similarity. The patch-level local depth loss is then computed as a normalized mean squared error (MSE) between corresponding patches:

$$\mathcal{L}_{local}^s = \frac{1}{K} \sum_{k=1}^K \|\hat{\mathbf{x}}_k^r - \hat{\mathbf{x}}_k^m\|_2^2.$$

3.3.2 Global Normalization. To complement the localized focus, we also incorporate global normalization, which enforces consistency in relative depth scale across the entire image. Instead of using per-patch statistics, we normalize each patch using a shared global standard deviation computed over the entire depth map:

$$\sigma_{global}^r = \text{std}(D_{rendered}), \quad \sigma_{global}^m = \text{std}(D_{mono}),$$

$$\tilde{\mathbf{x}}_k^r = \frac{\mathbf{x}_k^r - \mu(\mathbf{x}_k^r)}{\sigma_{global}^r + \epsilon}, \quad \tilde{\mathbf{x}}_k^m = \frac{\mathbf{x}_k^m - \mu(\mathbf{x}_k^m)}{\sigma_{global}^m + \epsilon}.$$

This formulation preserves scene-level depth relationships and mitigates inconsistencies in global geometry. The global depth loss is similarly computed as:

$$\mathcal{L}_{\text{global}}^s = \frac{1}{K} \sum_{k=1}^K \|\tilde{\mathbf{x}}_k^r - \tilde{\mathbf{x}}_k^m\|_2^2.$$

3.3.3 Multi-Scale Aggregation. To fully exploit depth cues at multiple spatial frequencies, we combine both local and global losses at each scale s using a weighted sum:

$$\mathcal{L}_{\text{depth}}^s = w_{\text{local}} \cdot \mathcal{L}_{\text{local}}^s + w_{\text{global}} \cdot \mathcal{L}_{\text{global}}^s.$$

Finally, we average the aggregated losses across all scales to obtain the total hierarchical depth supervision objective:

$$\mathcal{L}_{\text{depth}} = \frac{1}{|S|} \sum_{s \in S} \mathcal{L}_{\text{depth}}^s.$$

This design provides the network with supervision signals that are both spatially adaptive and scale-aware. While local normalization guides the model to match fine-grained structures, global normalization encourages coherent geometry across broader spatial contexts. Together, they enable the model to refine both macro-level scene layout and micro-level surface details, significantly improving reconstruction fidelity in sparse-view conditions.

3.4 Cascade Pearson Correlation Loss

Although hierarchical depth supervision provides rich multi-scale guidance, directly aligning the monocular depth with rendered depth from 3DGS remains a challenging task due to inherent inconsistencies in scale. Monocular depth predictions are typically uncalibrated and may differ significantly in magnitude from the metric scale depths rendered by 3D Gaussian Splatting. As a result, standard distance-based losses such as ℓ_1 and ℓ_2 become unreliable, as they penalize absolute differences and fail to capture structural similarity under scale mismatch.

To address this limitation, we introduce the use of the Pearson correlation coefficient as a scale-invariant loss function for depth alignment. Unlike traditional regression losses, Pearson correlation captures the relative structural similarity between signals by normalizing away both mean and variance. Given a rendered depth patch $D_r = \{d_r^i\}_{i=1}^N$ and a corresponding monocular depth patch $D_m = \{d_m^i\}_{i=1}^N$, the Pearson correlation loss is computed as:

$$\mathcal{L}_{\text{PCC}} = 1 - \frac{\sum_{i=1}^N (d_r^i - \bar{d}_r)(d_m^i - \bar{d}_m)}{\sqrt{\sum_{i=1}^N (d_r^i - \bar{d}_r)^2} \cdot \sqrt{\sum_{i=1}^N (d_m^i - \bar{d}_m)^2}},$$

where $\bar{d}_r = \frac{1}{N} \sum_{i=1}^N d_r^i$ and $\bar{d}_m = \frac{1}{N} \sum_{i=1}^N d_m^i$ represent the mean values of the rendered and monocular patches, respectively. This formulation encourages alignment of structural gradients and relative depth ordering, while remaining invariant to scale and offset, making it well-suited for monocular supervision.

To further enhance supervision, we propose the *Cascade Pearson Correlation (CPC)* strategy, which applies the Pearson loss across multiple spatial granularities. Instead of computing the correlation

over a single resolution, CPC enforces structural consistency hierarchically—at the global image level, over regional mid-sized patches, and within fine-grained local patches. Each level captures different frequencies of depth variation, enabling the model to iteratively refine geometry from coarse layout to fine surface detail.

The final cascade loss integrates these multi-scale signals into a unified objective:

$$\mathcal{L}_{\text{CPC}} = \alpha \mathcal{L}_{\text{PCC}}^{\text{global}} + \beta \mathcal{L}_{\text{PCC}}^{\text{regional}} + \gamma \mathcal{L}_{\text{PCC}}^{\text{local}},$$

where α, β, γ are scalar weights that balance the contribution from each scale. The hierarchical design ensures that depth supervision is effective at multiple abstraction levels—scene-wide consistency, object-level structure, and local surface detail.

By combining hierarchical depth supervision with scale-invariant CPC loss, our framework provides strong and consistent guidance across spatial hierarchies. This results in improved geometric fidelity and sharper reconstructions under sparse input views, effectively overcoming the limitations of absolute losses and enabling reliable optimization even in the presence of scale ambiguity.

3.5 Dense Initialization via VGGsFM

Previous 3DGS-based methods typically rely on traditional Structure-from-Motion (SfM) techniques to initialize the 3D point cloud. However, under sparse-view conditions, these methods often yield noisy or insufficient reconstructions due to limited feature correspondences.

To overcome this, we adopt VGGsFM, a learning-based SfM method that integrates classical multi-view geometry with VGG-based deep feature descriptors for robust and dense matching. Given a set of training views $\mathcal{V} = \{V_i = (I_i, P_i)\}_{i=1}^M$, where I_i denotes the input image and $P_i \in SE(3)$ is the camera pose, we extract deep local features as $F_i = f(I_i)$ using a pre-trained VGG network.

Dense pairwise feature matching is performed between image pairs (I_i, I_j) , resulting in a set of matched keypoints:

$$\mathcal{M}_{i,j} = \{(\mathbf{p}_i^k, \mathbf{p}_j^k)\}_{k=1}^{K_{ij}}.$$

These matches are triangulated into 3D coordinates using multi-view geometry:

$$\mathbf{X}_l = \text{Triangulate}(\mathbf{p}_i^k, \mathbf{p}_j^k, P_i, P_j), \quad \forall (\mathbf{p}_i^k, \mathbf{p}_j^k) \in \mathcal{M}_{i,j}.$$

The resulting 3D points are aggregated into a candidate point cloud:

$$\mathcal{P}_{\text{VGGsFM}} = \{\mathbf{X}_l\}_{l=1}^L.$$

To refine this reconstruction, VGGsFM incorporates confidence-based filtering, which discards 3D points with low photometric or geometric consistency. The filtered set

$$\mathcal{P}_{\text{init}} = \{\mathbf{X}_l\}_{l=1}^{L'}, \quad \text{with } L' < L,$$

serves as the initialization for the 3D Gaussians. Specifically, each 3D Gaussian is initialized with a center $\mu_l := \mathbf{X}_l$.

This dense and reliable initialization enhances the stability and convergence of subsequent optimization in sparse-view 3D Gaussian Splatting.

Table 1: Quantitative results on DTU[12] and LLFF[20] with 3 input views.

Method	Setting	DTU			LLFF		
		PSNR \uparrow	SSIM \uparrow	LPIPS \downarrow	PSNR \uparrow	SSIM \uparrow	LPIPS \downarrow
SRF[7]	Trained on DTU	15.32	0.671	0.304	12.34	0.250	0.591
PixelNeRF[41]		16.82	0.695	0.270	7.93	0.272	0.682
MVSNeRF[3]		18.63	0.769	0.197	17.25	0.557	0.356
Mip-NeRF[1]	Optimized per Scene	8.68	0.571	0.353	14.62	0.351	0.495
DietNeRF[11]		11.85	0.633	0.314	14.94	0.370	0.496
RegNeRF[23]		18.89	0.745	0.190	19.08	0.587	0.336
FreeNeRF[38]		19.92	0.787	0.182	19.63	0.612	0.308
SparseNeRF[32]		19.55	0.769	0.201	19.86	0.624	0.328
3DGS[14]	3DGS-based Methods	13.38	0.614	0.356	15.52	0.482	0.370
DRGS[8]		-	-	-	17.17	0.497	0.337
SparseGS[35]		18.89	0.702	0.229	-	-	-
DNGaussian[16]		18.23	0.780	0.184	18.86	0.600	0.294
FSGS[45]		-	-	-	20.43	0.682	0.248
MVPGS[37]		<u>20.50</u>	<u>0.871</u>	0.106	20.39	<u>0.715</u>	<u>0.203</u>
SCGaussian[25]		-	-	-	<u>20.77</u>	0.705	0.218
FewViewGS[40]		19.74	0.861	0.127	20.54	0.693	0.214
HDGS (Ours)		21.45	0.874	<u>0.108</u>	20.91	0.735	0.180

4 Experiment

4.1 Datasets

We conduct experiments on two real-world datasets, DTU[12] and LLFF[20], both of which are standard benchmarks for evaluating novel view synthesis methods.

4.1.1 LLFF. This dataset consists of real-world forward-facing indoor and outdoor scenes, characterized by diverse geometry and photometric complexity. Following prior works, we use every eighth image as the test set, while training views are uniformly sampled from the remaining images. We apply the same sparse view sampling strategy using three training views and downsample all images by a factor of 8 (378x504) to balance computational efficiency and reconstruction quality.

4.1.2 DTU. This dataset contains 124 indoor object-centric scenes captured in a controlled laboratory environment. The DTU dataset comprises a total of 124 indoor object-centric scenes. In line with previous works [10, 16], we select 15 representative scenes for evaluation, with the following IDs: 1, 2, 9, 10, 11, 12, 14, 15, 23, 24, 26, 27, 29, 30, 31, 32, 33, 34, 35, 41, 42, 43, 45, 46, 47. During testing, the background is removed using provided masks to focus the evaluation on the reconstruction quality of the foreground object. All images are downsampled by a factor of 4, resulting in a resolution of 300x400. We adopt the same sparse-view configuration as in LLFF, using three input views per scene during training.

4.2 Evaluation Metrics

For quantitative evaluation, we adopt three common metrics: Peak Signal-to-Noise Ratio (PSNR), Structural Similarity Index (SSIM),

and Learned Perceptual Image Patch Similarity (LPIPS). PSNR and SSIM are metrics where higher values indicate better results, measuring pixel-level accuracy and structural resemblance, respectively. In contrast, LPIPS is a perceptual metric, with lower values indicating better perceptual similarity.

4.3 Implementation Details

Our method is implemented in PyTorch with CUDA acceleration and is developed on top of the publicly available gsplat v1.3 framework[39]. All experiments are conducted using an NVIDIA A6000 GPU.

For dense initialization, we employ a pre-trained VGGSfM model to generate 3D point clouds from matched keypoints across the input views. This initialization provides denser and more reliable geometric supervision, particularly beneficial under sparse-view conditions. We utilize DPT[27] to generate monocular depth.

All scenes in the LLFF and DTU datasets are trained for 30,000 iterations. During training, we apply hierarchical depth supervision by incorporating both local and global depth consistency into the loss function. The local loss is computed as a weighted sum of Pearson correlation loss ($w_p = 0.1$) and L2 loss ($w_{l2} = 0.9$), with the same weighting applied to the global loss. These two components are then combined using weights $w_{\text{local}} = 0.7$ and $w_{\text{global}} = 0.3$. The resulting hierarchical depth loss is integrated into the final loss function with a depth supervision weight of $\lambda = 5 \times 10^{-3}$.

4.4 Baselines

We compare our proposed approach against several state-of-the-art methods in sparse-view novel view synthesis. For NeRF-based methods, we select SRF[7], PixelNeRF[41], MVSNeRF[3], Mip-NeRF[1],

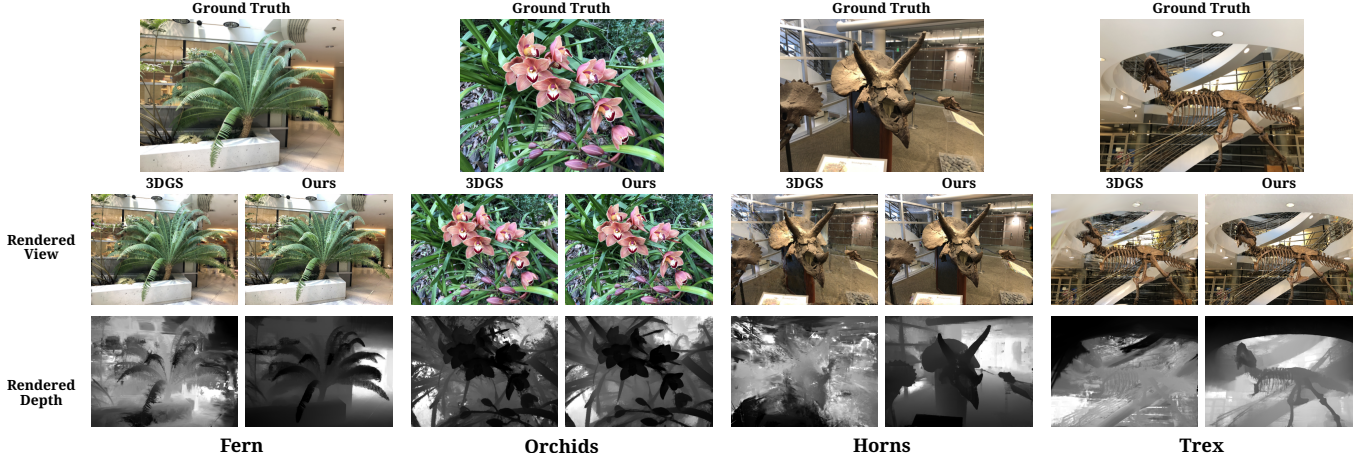


Figure 2: Qualitative comparison of rendered RGB images and depth maps on the LLFF dataset using 3 input views

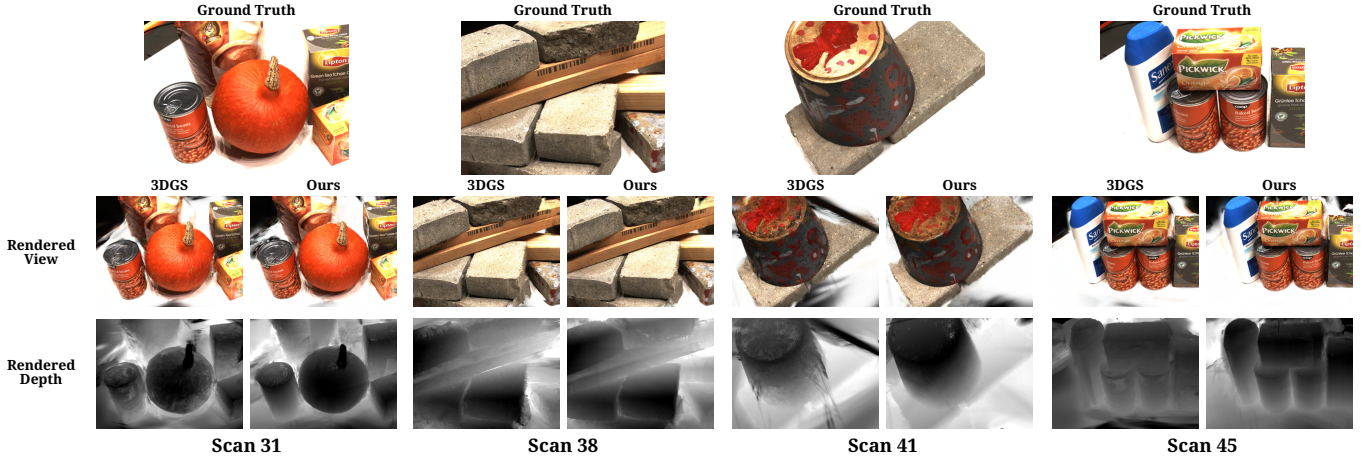


Figure 3: Qualitative comparison of rendered RGB images and depth maps on the DTU dataset using 3 input views

DietNeRF[11], RegNeRF[23], FreeNeRF[38], SparseNeRF[32], as baseline comparisons, given their established performance in sparse-view scenarios. For 3D Gaussian Splatting-based methods, we benchmark against DRGS[8], SparseGS[35], DNGaussian[16], FSGS[45], MVPGS[37], SCGaussian[25], FewViewGS[40] and the original 3DGS[14] implementation. These methods provide comprehensive baselines that evaluate both implicit volumetric and explicit representation-based synthesis under challenging sparse-view conditions.

4.5 Qualitative Results

As shown in Figure 2 and Figure 3, we evaluate our method under the sparse-view setting on two benchmarks: LLFF and DTU. All scenes are trained for 30000 iterations using only 3 input views. LLFF contains real-world forward-facing scenes with complex textures and backgrounds, while DTU focuses on object-centric reconstructions. We compare our method against the baseline 3D Gaussian Splatting (3DGS), using both quantitative metrics and

visual quality. Our approach demonstrates superior rendering fidelity and geometric consistency across both datasets. Below, we highlight key improvements in representative scenes.

4.5.1 LLFF. In the Fern scene, baseline 3DGS exhibits blurry foliage and color bleeding in regions with overlapping leaves. Our method produces sharper leaf contours and better depth layering, effectively separating foreground and background structures. In Orchids, the baseline fails to recover thin flower stems and introduces distortions around petal edges. In contrast, our approach preserves delicate structures and renders cleaner color transitions, owing to multi-scale depth alignment. In the Horns scene, the antlers suffer from severe smoothing in the baseline result, blending into the background. Our method retains their curved and branched geometry with minimal distortion. For the Trex scene, the baseline output introduces ghosting and blurred outlines around the dinosaur’s limbs. Our reconstruction captures clear silhouettes, sharper textures, and better separation between the model and background foliage.

4.5.2 DTU. In Scan 31, which includes thin metal structures and complex occlusions, the baseline produces soft, distorted edges. Our method reconstructs thin rods and layered geometry with high fidelity. In Scan 38, the baseline suffers from shape flattening and over-smoothing around detailed surface regions. Our model preserves sharper surface contours and more accurate shading transitions. In Scan 41, where depth discontinuities are prominent, our approach reduces blending artifacts and recovers stronger depth contrast between object parts. Finally, in Scan 45, the baseline exhibits color spill and warped geometry near occlusion boundaries. Our method generates cleaner edges and maintains structural coherence across depth layers. These results confirm the effectiveness of our hierarchical depth supervision and cascade correlation loss.

4.6 Ablation study

We evaluate the contribution of each key component in our proposed method through an ablation study on the LLFF dataset. Specifically, we analyze the impact of Dense Initialization (DI), Pearson Correlation (PC) loss, the Linear Kernel (LK), and Hierarchical Depth (HD) supervision. Quantitative results are presented in Table 2 and Table 3.

4.6.1 Impact of key components. Table 2 shows the performance of our system when individual components are introduced incrementally. The first row reports the baseline results of 3DGS under sparse-view settings, serving as our reference.

We begin by introducing DI, which replaces the sparse SfM-based point cloud with a denser initialization from VGGSfM. While DI alone yields moderate improvements, its benefits become more evident when combined with additional supervision.

Incorporating PC loss alongside DI consistently enhances all evaluation metrics. This suggests that enforcing structural consistency through correlation provides meaningful geometric guidance. Replacing standard correlation with HD supervision further boosts performance, highlighting the advantage of aligning depth across multiple spatial scales. When HD and PC are used jointly, we observe even stronger results, thus demonstrating their complementary contributions.

A similar trend emerges with the introduction of the Linear Kernel (LK). By preserving local details and sharp boundaries more effectively under sparse input conditions, LK further improves rendering accuracy. The full model, which integrates DI, LK, HD, and PC, achieves the highest performance across all metrics—showcasing the cumulative benefits of each component in enhancing geometric fidelity and rendering quality.

4.6.2 Effect of Patch Configurations. To better understand the contribution of hierarchical depth supervision, we conduct experiments using different patch scale configurations within the HD+PC module. Specifically, we examine the effect of varying the number and size of patches used during training by testing four configurations: a single-scale setup with patch size 4, a two-scale setup with patch sizes 4 and 8, a three-scale setup with patch sizes 4, 8, and 16, and a four-scale setup with patch sizes 4, 8, 16, and 32.

The quantitative results, reported in Table 3, show a clear trend: model performance improves progressively as additional scales are introduced, with the best results achieved using the three-scale

Table 2: Ablation study of individual components, including Hierarchical Depth (HD) supervision, Pearson Correlation (PC) loss, Linear Kernel (LK), and Dense Initialization (DI), on the LLFF dataset.

Method	PSNR \uparrow	SSIM \uparrow	LPIPS \downarrow
3DGS	15.52	0.482	0.370
DI	18.16	0.620	0.285
DI + PC	18.728	0.647	0.246
DI + HD	18.93	0.664	0.227
DI + HD + PC	18.95	0.667	0.226
DI + LK	19.89	0.687	0.236
DI + LK + PC	20.00	0.696	0.213
DI + LK + HD	20.77	0.727	0.184
DI + LK + HD + PC	20.91	0.735	0.180

Table 3: Quantitatively ablation for different patch size configuration on LLFF dataset.

Method	PSNR \uparrow	SSIM \uparrow	LPIPS \downarrow
4	20.76	0.731	0.181
4+8	20.77	0.728	0.182
4+8+16	20.91	0.735	0.180
4+8+16+32	20.74	0.725	0.185

configuration (4+8+16). This pattern highlights the importance of supervising depth alignment at multiple spatial resolutions. Fine-scale patches (e.g., size 4) are effective at capturing local surface variation and edge-level details, while mid-scale patches (e.g., size 8 and 16) contribute broader structural context, allowing the model to align depth gradients over larger spatial regions.

The inclusion of multiple scales enables the model to simultaneously focus on preserving local detail and ensuring global coherence, leading to improved depth prediction and rendering accuracy. However, when an even coarser patch size of 32 is added, a slight drop in performance is observed. We attribute this to the diminished discriminative power of very large patches, which average out fine geometric variation and introduce redundancy in supervision. Large patches may also span semantically or structurally inconsistent regions, making correlation-based alignment less meaningful and potentially noisy.

Overall, these results justify our choice of using a three-level hierarchy for HD and PC. This configuration offers a balanced trade-off between local and global supervision, capturing depth structure across multiple spatial frequencies without overwhelming the network with overly coarse or redundant information. This validates our hierarchical design as an effective strategy for guiding geometry learning in sparse-view scenarios.

5 Conclusion

In this paper, we propose Hierarchical Depth Guided Sparse-View 3D Gaussian Splatting, an advanced method designed to significantly enhance the performance of novel view synthesis under sparse-view scenarios. We introduce a hierarchical depth supervision strategy that integrates monocular depth priors across multiple spatial granularities, ensuring precise Gaussian distribution across

global, regional, and local scales. Furthermore, our Cascade Pearson Correlation loss robustly aligns rendered depth with monocular depth estimates at all hierarchical levels, effectively addressing scale inconsistencies inherent in monocular depth predictions. By leveraging linear kernel-based splatting, our approach effectively mitigates detail loss typically caused by conventional Gaussian kernels, thus preserving local geometric sharpness. Through a dense initialization strategy utilizing the VGGsFM model, our method achieves stable optimization and enhanced reconstruction fidelity. Comprehensive experiments on standard benchmarks demonstrate that our method outperforms current state-of-the-art approaches, delivering superior rendering quality and robustness in sparse-view settings.

References

- [1] Jonathan T Barron, Ben Mildenhall, Matthew Tancik, Peter Hedman, Ricardo Martin-Brualla, and Pratul P Srinivasan. 2021. Mip-nerf: A multiscale representation for anti-aliasing neural radiance fields. In *Proceedings of the IEEE/CVF international conference on computer vision*. 5855–5864.
- [2] Jonathan T Barron, Ben Mildenhall, Dor Verbin, Pratul P Srinivasan, and Peter Hedman. 2022. Mip-nerf 360: Unbounded anti-aliased neural radiance fields. In *Proceedings of the IEEE/CVF conference on computer vision and pattern recognition*. 5470–5479.
- [3] Anpei Chen, Zexiang Xu, Fuqiang Zhao, Xiaoshuai Zhang, Fanbo Xiang, Jingyi Yu, and Hao Su. 2021. Mvsnerf: Fast generalizable radiance field reconstruction from multi-view stereo. In *Proceedings of the IEEE/CVF international conference on computer vision*. 14124–14133.
- [4] Guikun Chen and Wenguan Wang. 2024. A Survey on 3D Gaussian Splatting. *arXiv preprint arXiv:2401.03890* (2024).
- [5] Haodong Chen, Runnan Chen, Qiang Qu, Zhaoqing Wang, Tongliang Liu, Xiaoming Chen, and Yuk Ying Chung. 2024. Beyond Gaussians: Fast and High-Fidelity 3D Splatting with Linear Kernels. *arXiv preprint arXiv:2411.12440* (2024).
- [6] Huan Chen, Cheng Li, and Gim Hee Lee. 2023. NeuSG: Neural Implicit Surface Reconstruction with 3D Gaussian Splatting Guidance. *arXiv preprint arXiv:2312.00846* (2023).
- [7] Julian Chibane, Aayush Bansal, Verica Lazova, and Gerard Pons-Moll. 2021. Stereo radiance fields (srf): Learning view synthesis for sparse views of novel scenes. In *Proceedings of the IEEE/CVF Conference on Computer Vision and Pattern Recognition*. 7911–7920.
- [8] Jaeyoung Chung, Jeongtaek Oh, and Kyoung Mu Lee. 2024. Depth-regularized optimization for 3d gaussian splatting in few-shot images. In *Proceedings of the IEEE/CVF Conference on Computer Vision and Pattern Recognition*. 811–820.
- [9] Sara Fridovich-Keil, Giacomo Meanti, Frederik Rahbæk Warburg, Benjamin Recht, and Angjoo Kanazawa. 2023. K-planes: Explicit radiance fields in space, time, and appearance. In *Proceedings of the IEEE/CVF Conference on Computer Vision and Pattern Recognition*. 12479–12488.
- [10] Liang Han, Junsheng Zhou, Yu-Shen Liu, and Zhizhong Han. 2024. Binocular-guided 3d gaussian splatting with view consistency for sparse view synthesis. *arXiv preprint arXiv:2410.18822* (2024).
- [11] Ajay Jain, Matthew Tancik, and Pieter Abbeel. 2021. Putting nerf on a diet: Semantically consistent few-shot view synthesis. In *Proceedings of the IEEE/CVF International Conference on Computer Vision*. 5885–5894.
- [12] Rasmus Jensen, Anders Dahl, George Vogiatzis, Engin Tola, and Henrik Aanæs. 2014. Large scale multi-view stereopsis evaluation. In *Proceedings of the IEEE conference on computer vision and pattern recognition*. 406–413.
- [13] Kai Katsumata, Duc Minh Vo, and Hideki Nakayama. 2024. A compact dynamic 3d gaussian representation for real-time dynamic view synthesis. In *European Conference on Computer Vision*. Springer, 394–412.
- [14] Bernhard Kerbl, Georgios Kopanas, Thomas Leimkühler, and George Drettakis. 2023. 3d gaussian splatting for real-time radiance field rendering. *ACM Trans. Graph.* 42, 4 (2023), 139–1.
- [15] Injae Kim, Minhyuk Choi, and Hyunwoo J. Kim. 2023. UP-NeRF: Unconstrained Pose-Prior-Free Neural Radiance Fields. In *Advances in Neural Information Processing Systems (NeurIPS)*. <https://arxiv.org/abs/2311.03784>
- [16] Jiahe Li, Jiawei Zhang, Xiao Bai, Jin Zheng, Xin Ning, Jun Zhou, and Lin Gu. 2024. Dngaussian: Optimizing sparse-view 3d gaussian radiance fields with global-local depth normalization. In *Proceedings of the IEEE/CVF conference on computer vision and pattern recognition*. 20775–20785.
- [17] Jonathon Luiten, Georgios Kopanas, Bastian Leibe, and Deva Ramanan. 2024. Dynamic 3d gaussians: Tracking by persistent dynamic view synthesis. In *2024 International Conference on 3D Vision (3DV)*. IEEE, 800–809.
- [18] Xiaoyang Lyu, Yang-Tian Sun, Yi-Hua Huang, Xiuzhe Wu, Ziyi Yang, Yilun Chen, Jiangmiao Pang, and Xiaojuan Qi. 2024. 3dgsr: Implicit surface reconstruction with 3d gaussian splatting. *ACM Transactions on Graphics (TOG)* 43, 6 (2024), 1–12.
- [19] Jinjie Mai, Wenxuan Zhu, Sara Rojas, Jesus Zarzar, Abdullah Hamdi, Guocheng Qian, Bing Li, Silvio Giancola, and Bernard Ghanem. 2024. TrackNeRF: Bundle Adjusting NeRF from Sparse and Noisy Views via Feature Tracks. In *Proceedings of the European Conference on Computer Vision (ECCV)*. Springer, 470–489. doi:10.1007/978-3-031-73254-6_27
- [20] Ben Mildenhall, Pratul P Srinivasan, Rodrigo Ortiz-Cayon, Nima Khademi Kalantari, Ravi Ramamoorthi, Ren Ng, and Abhishek Kar. 2019. Local light field fusion: Practical view synthesis with prescriptive sampling guidelines. *ACM Transactions on Graphics (ToG)* 38, 4 (2019), 1–14.
- [21] Ben Mildenhall, Pratul P Srinivasan, Matthew Tancik, Jonathan T Barron, Ravi Ramamoorthi, and Ren Ng. 2021. Nerf: Representing scenes as neural radiance fields for view synthesis. *Commun. ACM* 65, 1 (2021), 99–106.
- [22] Thomas Müller, Alex Evans, Christoph Schied, and Alexander Keller. 2022. Instant neural graphics primitives with a multiresolution hash encoding. *ACM Trans. Graph.* 41, 4, Article 102 (July 2022), 15 pages. doi:10.1145/3528223.3530127

- [23] Michael Niemeyer, Jonathan T Barron, Ben Mildenhall, Mehdi SM Sajjadi, Andreas Geiger, and Noha Radwan. 2022. Regnerf: Regularizing neural radiance fields for view synthesis from sparse inputs. In *Proceedings of the IEEE/CVF conference on computer vision and pattern recognition*. 5480–5490.
- [24] Avinash Paliwal, Wei Ye, Jinhui Xiong, Dmytro Kotovenko, Rakesh Ranjan, Vikas Chandra, and Nima Khademi Kalantari. 2024. Coherentgs: Sparse novel view synthesis with coherent 3d gaussians. In *European Conference on Computer Vision*. Springer, 19–37.
- [25] Rui Peng, Wangze Xu, Luyang Tang, Jianbo Jiao, Ronggang Wang, et al. 2024. Structure consistent gaussian splatting with matching prior for few-shot novel view synthesis. *Advances in Neural Information Processing Systems* 37 (2024), 97328–97352.
- [26] Albert Pumarola, Enric Corona, Gerard Pons-Moll, and Francesc Moreno-Noguer. 2021. D-nerf: Neural radiance fields for dynamic scenes. In *Proceedings of the IEEE/CVF conference on computer vision and pattern recognition*. 10318–10327.
- [27] René Ranftl, Alexey Bochkovskiy, and Vladlen Koltun. 2021. Vision transformers for dense prediction. In *Proceedings of the IEEE/CVF international conference on computer vision*. 12179–12188.
- [28] Brandon Smart, Chuanxia Zheng, Iro Laina, and Victor Adrian Prisacariu. 2024. Splatt3r: Zero-shot gaussian splatting from uncalibrated image pairs. *arXiv preprint arXiv:2408.13912* (2024).
- [29] Lisong C Sun, Neel P Bhatt, Jonathan C Liu, Zhiwen Fan, Zhangyang Wang, Todd E Humphreys, and Ufuk Topcu. 2024. Mm3dgs slam: Multi-modal 3d gaussian splatting for slam using vision, depth, and inertial measurements. In *2024 IEEE/RSJ International Conference on Intelligent Robots and Systems (IROS)*. IEEE, 10159–10166.
- [30] Shengji Tang, Weicai Ye, Peng Ye, Weihao Lin, Yang Zhou, Tao Chen, and Wanli Ouyang. 2024. Hisplat: Hierarchical 3d gaussian splatting for generalizable sparse-view reconstruction. *arXiv preprint arXiv:2410.06245* (2024).
- [31] Prune Truong, Marie-Julie Rakotosaona, Fabian Manhardt, and Federico Tombari. 2023. SPARF: Neural Radiance Fields From Sparse and Noisy Poses. In *Proceedings of the IEEE/CVF Conference on Computer Vision and Pattern Recognition (CVPR)*. 4190–4200.
- [32] Guangcong Wang, Zhaoxi Chen, Chen Change Loy, and Ziwei Liu. 2023. Sparsenerf: Distilling depth ranking for few-shot novel view synthesis. In *Proceedings of the IEEE/CVF international conference on computer vision*. 9065–9076.
- [33] Jianyuan Wang, Nikita Karaev, Christian Rupprecht, and David Novotny. 2024. Vggsfm: Visual geometry grounded deep structure from motion. In *Proceedings of the IEEE/CVF conference on computer vision and pattern recognition*. 21686–21697.
- [34] Tong Wu, Yu-Jie Yuan, Li-Xin Zhang, Jia Yang, Yuan-Peng Cao, Liang-Qun Yan, and Ling Gao. 2024. Recent Advances in 3D Gaussian Splatting. *Computational Visual Media* 10 (2024), 613–642.
- [35] Haolin Xiong. 2024. *SparseGS: Real-time 360° sparse view synthesis using Gaussian splatting*. University of California, Los Angeles.
- [36] Jiale Xu, Shenghua Gao, and Ying Shan. 2024. FreeSplat: Pose-free Gaussian Splatting for Sparse-view 3D Reconstruction. *arXiv preprint arXiv:2412.09573* (2024).
- [37] Wangze Xu, Huachen Gao, Shihe Shen, Rui Peng, Jianbo Jiao, and Ronggang Wang. 2024. Mvpgs: Excavating multi-view priors for gaussian splatting from sparse input views. In *European Conference on Computer Vision*. Springer, 203–220.
- [38] Jiawei Yang, Marco Pavone, and Yue Wang. 2023. Freenerf: Improving few-shot neural rendering with free frequency regularization. In *Proceedings of the IEEE/CVF conference on computer vision and pattern recognition*. 8254–8263.
- [39] Vickie Ye, Ruilong Li, Justin Kerr, Matias Turkulainen, Brent Yi, Zhuoyang Pan, Otto Seiskari, Jianbo Ye, Jeffrey Hu, Matthew Tancik, et al. 2025. gsplat: An open-source library for Gaussian splatting. *Journal of Machine Learning Research* 26, 34 (2025), 1–17.
- [40] Ruihong Yin, Vladimir Yugay, Yue Li, Sezer Karaoglu, and Theo Gevers. 2024. FewViewGS: Gaussian Splatting with Few View Matching and Multi-stage Training. *arXiv preprint arXiv:2411.02229* (2024).
- [41] Alex Yu, Vickie Ye, Matthew Tancik, and Angjoo Kanazawa. 2021. pixelnerf: Neural radiance fields from one or few images. In *Proceedings of the IEEE/CVF conference on computer vision and pattern recognition*. 4578–4587.
- [42] Jiawei Zhang, Jiahe Li, Xiaohan Yu, Lei Huang, Lin Gu, Jin Zheng, and Xiao Bai. 2024. CoR-GS: sparse-view 3D Gaussian splatting via co-regularization. In *European Conference on Computer Vision*. Springer, 335–352.
- [43] Wenyuan Zhang, Yu-Shen Liu, and Zhizhong Han. 2024. Neural signed distance function inference through splatting 3d gaussians pulled on zero-level set. *arXiv preprint arXiv:2410.14189* (2024).
- [44] Chen Zhao, Xuan Wang, Tong Zhang, Saqib Javed, and Mathieu Salzmann. 2024. Self-Ensembling Gaussian Splatting for Few-Shot Novel View Synthesis. *arXiv preprint arXiv:2411.00144* (2024).
- [45] Zehao Zhu, Zhiwen Fan, Yifan Jiang, and Zhangyang Wang. 2024. Fsgs: Real-time few-shot view synthesis using gaussian splatting. In *European conference on computer vision*. Springer, 145–163.